ACI STRUCTURAL JOURNAL TECHNICAL PAPER

Title No. 112-S67

Destructive Horizontal Load Tests of Full-Scale Recycled-Aggregate Concrete Structures

by João Pacheco, Jorge de Brito, João Ferreira, and Diogo Soares

A study regarding the structural behavior of four three-dimensional, full-scale, recycled-aggregate concrete frame structures was carried out. This paper describes the final tests, which consisted of destructive horizontal tests, with incremental monotonic loading, in accordance with a pushover analysis. The test structures had a varying content of coarse recycled aggregates (0%, 25%, 100%, and 100% with high-range water-reducing admixture—in overall volume of coarse aggregates). These aggregates were generated from the concrete precasting industry—that is, they are high quality and their negative effect on the recycled aggregate concrete mixtures was not expected to be significant. The four structures had the same geometry and reinforcement layout, and their design complied with Eurocode 2, Eurocode 7, and Eurocode 8. All the structures exhibited a ductile behavior, and their behavior was not significantly affected by the incorporation of recycled aggregates. There were also no differences in the cracking response. To the authors' best knowledge, this is the first time that such experiments were made in full-scale recycled-aggregate concrete structures.

Keywords: full-scale models; pushover; recycled-aggregate concrete; structural behavior; three-dimensional frame.

INTRODUCTION AND RESEARCH SIGNIFICANCE

The use of recycled aggregates (RA) in concrete is a step toward sustainability, enabling a reduction of the use of natural resources and of the waste produced. However, the structural behavior of structures made with RA has not been fully studied, especially concerning their seismic response.

To study the applicability of this kind of material by the construction industry, this experiment aims at assessing whether the performance of RA concrete (RAC) structures, when subjected to seismic actions, follows the assumptions made when designing conventional reinforced concrete structures.

Not only is the mechanical (linear and nonlinear) behavior of RAC structures evaluated, but also the use of the calculation methods employed in common concrete structures in this kind of material. This evaluation is made by the study of quantitative and qualitative parameters measured stage-by-stage during a monotonic destructive load application in compliance with the pushover analysis definition in Eurocode 8.

Additionally, because no full-scale studies regarding the behavior of RAC structures have been made, the evaluation of possible size effects is a necessary step toward the use of RAC (for instance, the ductility of a scaled-down specimen can overestimate the actual ductility of a structure, as argued by Bažant [1999]).

Other innovative aspects of this experiment are the use of RA from the precasting industry (thus, high quality is expected) and that, contrary to most studies, these structures were executed in a common construction environment, with choices made to comply with such working conditions (such as a simpler aggregate grading). Therefore, it can be stated that this study aims at replicating the performance of RAC structures as if they were built for common construction purposes, and not for research purposes.

The experiment also aimed at raising awareness and trust in the applicability of RA in concrete structures, providing an eco-friendly solution to precast rejects by confirming that the use of RA allows building reinforced concrete structures with an adequate seismic behavior.

Only the use of the coarse fraction of the recycled aggregates was considered because the fine fraction tends to have a higher percentage of attached mortar, thus resulting in a larger loss of durability and mechanical properties (González-Fonteboa and Martínez-Abella 2007; Sato et al. 2007).

LITERATURE REVIEW

General introduction

The main difference between conventional concrete (CC) and RAC is that RAC contains RAs, which are made of natural stone aggregates and mortar attached to them. The presence of this mortar has a series of implications on the behavior of RAC, mostly due to the higher porosity and permeability of this material: RAC tend to have higher water absorption; lower durability performance (Kwan et al. 2012; Olorunsogo and Padayachee 2002), which can be mitigated with fly ash (Kou et al. 2012); lower workability; and, most probably, lower mechanical performance, reflected mainly on a decrease of the Young's modulus E (Fonseca et al. 2011; Kou et al. 2012). Studies regarding shrinkage and creep show that these properties tend to increase with the use of RA (Ferreira et al. 2011; Poon et al. 2002).

Despite in some cases deteriorating the properties of concrete, the use of RA is not barred by this effect. Furthermore, the studies that compare RAC properties with regulations and engineering codes (Gonçalves and de Brito 2010) are almost unanimous in concluding their compliance.

ACI Structural Journal, V. 112, No. 6, November-December 2015.

MS No. S-2014-146.R4, doi: 10.14359/51687800, received November 24, 2014, and reviewed under Institute publication policies.

Additionally, the use of high-range water-reducing admixtures (HRWRAs) can offset part of these detrimental effects, notably in terms of concrete strength, modulus of elasticity, and splitting tensile strength (Barbudo et al. 2013; Matias et al. 2013; Pereira et al. 2012), mainly due to the higher compactability and lower *w*/*c* (for the same workability) achieved, despite Matias et al. (2013) stating that HRWRAs are more efficient in CC than in RAC.

Pereira et al. (2012) suggest such a decrease in HRWRA performance happens when its mechanism is based on electrostatic repulsion (as for HRWRAs based on lignosulfates with additions, the product used in the experiment of Matias et al. [2013]). Electrostatic repulsion is characterized by the development of negative charge on the cement particles (by adsorption of the HRWRA's agent), improving the fluidity of concrete by dispersing cement particles in the concrete paste, thus avoiding the formation of significant agglomerates of these particles. This process originates a small area surrounding the cement particle, characterized by a significantly negative zeta-potential value (Björnström and Chandra 2003). Because RAs contain attached mortar, part of the HRWRA is adsorbed by the RA instead of by the cement particles, reducing its efficiency.

High-range water-reducing admixtures based on polycarboxylic agents, as the one used in this experiment is, act mostly by steric hindrance (Yoshioka et al. 1997). This process is characterized by the extension of long hydrophilic draft chains of the polycarboxylic polymer away from the cement particles, which improve the workability of fresh concrete by Pauli/Born repulsion. This process is less dependent on the adsorption by RA, due to the "range" of these chains—that is, even if a given polycarboxylic chain is adsorbed by mortar attached to the recycled aggregate, the chain is still contributing to the steric hindrance effect. Therefore, a reduction of the efficiency of this kind of HRWRA associated with RA incorporation is not expected to be significant.

However, the effect of HRWRAs in RAC is a subject that has not yet been thoroughly studied and the authors emphasize that this possible explanation needs to be confirmed.

The effect of RA incorporation on the structural behavior of concrete is discussed in both Li (2009) and Xiao et al. (2012)—two different reviews that concern the behavior of RAC elements. Succinctly, the constitutive relations of RAC are similar to those of CC (Xiao et al. 2005) and the deflections increase in most of the references cited in this paragraph, due to the reduction in modulus of elasticity. The load capacity of beams subjected to bending (Sato et al. 2007; Li 2009) and beams subjected to shear (Li 2009; González-Fonteboa and Martínez-Abella 2007) depend mostly on the reinforcement of the elements tested, with reduced decreases caused by RA (typical differences between 3% and 7% in most of the studies cited, for total coarse replacement).

The cracking behavior of concrete structures has the same pattern, independently of RA use, despite Li (2009) stating that other researchers observed a higher crack width in mixtures with higher RA content. In compliance with these conclusions, González-Fonteboa and Martínez-Abella (2007) studied the shear behavior of RAC with different reinforcement layouts and witnessed an increase in crack width associated with RA incorporation; another conclusion of the study was that a reduced spacing between stirrups mitigates this effect. Xiao et al. (2012) state that Liu et al. studied columns whose cracking load decreased with RA incorporation. On the other hand, in Sato et al. (2007) the flexural behaviour of beams is studied and, for various incorporation ratios of recycled coarse aggregates, crack width and spacing were independent of RA use.

Studies of structures subjected to horizontal loads

There are few studies regarding the response of RAC structures, and most of them come from investigations made in the People's Republic of China and are not available in English.

The studies available in English show that the use of RA has no significant influence on the overall seismic behavior, as the examples given in Yang and Han (2006) and Xiao et al. (2012) suggest, with a decrease in load capacity, deformations, ductility, and energy dissipation associated with a total recycled coarse aggregate incorporation below 10% (columns subject to both pure and eccentric compression).

Corinaldesi et al. (2011) state that a good structural behavior of RAC column-beam joints is expected, despite suggesting that the actual RAC shear strength and stiffness should be considered in the structural design. Xiao et al. (2012) claim that column-beam joints behave sufficiently well, complying with Japanese standards, despite a slightly poorer performance for seismic actions.

Xiao et al. (2012) and Li (2009) made reviews of the experiments conducted in the People's Republic of China. For instance, Sun in 2006, cited by Li (2009), studied two-dimensional frames, witnessing a slight decrease in their load capacity associated with RA use, despite a good seismic response and only a negligible influence on the ductility. Bai et al., cited by Xiao et al. (2012), had similar findings, despite stating that a slight reduction in ductility was seen in structures with RA. Xiao et al. (2005) state that non-reinforced concrete ductility decreases with the use of RA due to the higher peak strain of RAC (caused by lower modulus of elasticity) and higher microcracking (due to an additional interface in the concrete microstructure between the original natural aggregates and the old mortar in RA). The main reason why the reduction in concrete ductility due to RA incorporation was only slightly noticed, or not noticed at all, in RAC structural elements is the presence of reinforcement steel.

Xiao et al. (2006) studied four 1:2 scaled bidimensional frames, with varying RA content, claiming that not only the same behavior was witnessed, but also that the differences in ductility, energy dissipation, loading stages, and deformations of the different structures (including one made with a reference mixture) were not significant despite increasing with RA incorporation—relative differences between CC and RAC with total replacement of the coarse fraction below 2% (6% for deformations).

Wang and Xiao (2013) tested the behavior of a single three-dimensional 1:4-scaled RAC structure in a shaking table. The structure behaved like a conventional concrete

Table 1—Concrete mixture composition, kg/m³ of concrete

Material		Concrete mixture			
		REF	B25	B100	B100SP
Fine sand		243.4	243.8	245.1	258.8
Coarse sand		448.4	448.8	450.12	475.5
Coarse natural aggregates	4 to 11.2 mm	437.4	328.1	0	0
	11.2 to 22.4 mm	666.8	500.1	0	0
Coarse recycled aggregates	4 to 10 mm	0	83.3	333.3	352.0
	10 to 20 mm	0	171.0	683.8	722.3
CEM II A-L 42.5R cement		350	350	350	350
Tap water		185.5	194.0	206.4	159.2
High-range water-reducing admixture		0	0	0	3.5
Effective *w*/*c*		0.53	0.54	0.54	0.40
Apparent *w*/*c*		0.53	0.55	0.59	0.45

Notes: Water content of HRWRA was not considered in definition of *w*/*c*; 1 kg = 2.20 lb; 1 m = 3.28 ft; 1 mm = 0.0394 in.

Table 2—Properties of concrete mixtures

	Density		Compressive strength						Splitting tensile strength		Elastic modulus		Ultrasonic pulse velocity	
			7-day			28-day			28-day					
Mixture	kg/m³	slugs/ft	MPa	psi	D_{REF}, %	MPa	psi	D_{REF}, %	MPa	psi	GPa	ksi	km/s	mi/s
REF	2377	148.32	39.2	5685.5	—	43.1	6251.1	—	3.1	449.6	36.2	5.25	4.71	2.93
B25	2344	146.27	38.2	5540.4	–2.55	44.6	6468.7	3.48	2.9	420.6	34.1	4.95	4.65	2.89
B100	2278	142.15	37.5	5438.9	–4.34	46.4	6729.7	7.66	3.1	449.6	32.1	4.66	4.42	2.75
B100SP	2410	150.38	60.6	8789.3	54.59	71.2	10326.7	65.2	4.3	623.7	39.5	5.73	4.70	2.92

structure, despite larger interstory deformations than those prescribed by regulations. It withstood a strong seismic action and the authors claimed that the structure showed good ductility.

Notwithstanding the studies reported, to the authors' best knowledge, this is the first study available regarding the behavior of full-scale three-dimensional RAC structures.

EXPERIMENTAL PLAN

Materials

Natural aggregates (NAs) and recycled coarse aggregates (RAs) were used. The NAs used were limestone coarse gravel and river sand. The recycled aggregates came from concrete blocks used in the pre-fabrication industry as support for long-span beams, with compressive strength above 7250 psi (50 MPa). These concrete blocks were processed in a crushing plant, producing aggregates with a proper grading (maximum aggregate dimension of 0.787 in. [20 mm]). To remove the dust produced during crushing, at the end of their production, the aggregates were flooded with water. The HRWRA used in this campaign had a polycarboxylic-based composition.

Composition of concrete mixtures

The objective was to develop concrete mixtures within Eurocode 2's Class C25/30. Prior to defining the four mixtures, compressive strength tests were made in several concrete mixtures produced in laboratory conditions with the aim of determining a mixture with the highest possible RA content but without significantly decreasing the resulting concrete's strength, and a mixture with a feasible content of HRWRA that maximized the gains in compressive strength, for total replacement of the coarse aggregates. The other two mixtures were a reference mixture of CC (REF) and a mixture in which all coarse aggregates are RA and no HRWRA is used (B100).

Due to the high quality of the RA coming from precast elements, it was found that, in fact, concrete strength slightly increased with the ratio of RA. Hence, the four mixtures used in this campaign were as follows: REF—reference mixture; B25—a mixture with the maximum ratio (25%) of RA allowed by the Portuguese Laboratory of Civil Engineering (LNEC E 471, 2006) and other institutions (Gonçalves and de Brito 2010), with the intent of replicating the properties of a conventional concrete; B100—mixture with full replacement of the coarse natural aggregates; and B100SP—a mixture similar to the previous one but with 1% HRWRA by cement weight. Table 1 contains the composition of each of these four mixtures. The distinction between "apparent" and "effective" water-cement ratio (*w*/*c*), shown in Table 1, is due to the water absorbed by the RA during mixing. This value is estimated in the laboratory by determining the water absorption and humidity content of RA.

Table 2 presents some of the laboratory properties of the concrete mixtures. Soares et al. (2014) present the properties of the RA. All the mixtures were complied with the target

slump of 125 ± 15 mm (4.92 ± 0.59 in.)—within EN 206-1's (2000) S3 slump class.

The use of a HRWRA produces concrete with a different *w*/*c* and cement matrix, implying that a comparison between mixtures with different mesostructures is made. This should be considered when comparing the results between concrete mixtures and is justified by the scope of this study (the viability of incorporating these RA in concrete, rather than the comparison between concrete mixtures with similar cementitious matrixes).

The aggregate grading followed a request from the construction company that supported this project, based on practicability on site: the difference in maximum size between the NA and the RA was due to the crushing process and the impracticability of sieving the natural aggregates.

The reinforcement steel used was A500, with B class of ductility.

Definition of test setup

The structures were tested individually, with a controlled load distribution.

After considering costs, maneuverability, and portability of the equipment to be used in this experiment, it was decided to apply the forces to the structures using grip hoists, with their cables attached to the column-beam joints, as shown in Fig. 1. Most of the remaining elements of the test setup are also shown, as well as the topographic targets used to measure displacements. The four anchor points (only two are shown) were attached to a concrete anchor block, represented in Fig. 2.

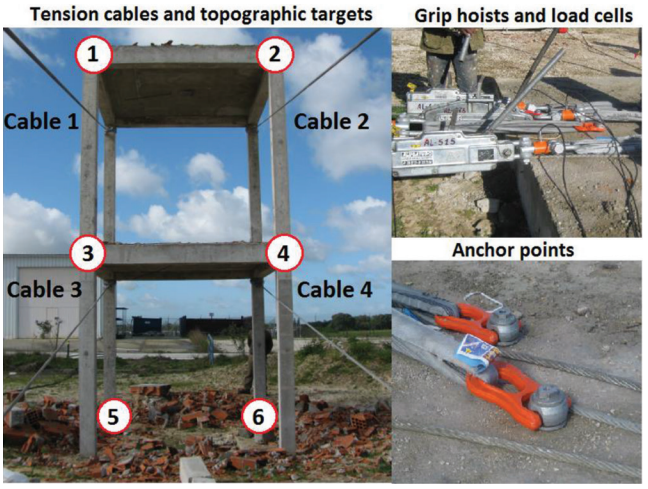

Fig. 1—Overview of test setup of one structure.

Due to the large scale of this project, it was necessary to design a test setup that would reuse materials and equipment, reducing costs and space required for the experiment. Hence, a cross-shaped solution was chosen. This solution only allows loading on one direction, emulating a pushover analysis whose loads are monotonic.

Because grip hoists were used to apply the loads, this experiment was a hybrid between force-controlled tests and deformation-controlled tests.

A load-controlled test would imply that, at any given stage of the experiment, the loads imposed on the structure would be controlled—that is, the input on the system would be the forces applied by each cable. On the other hand, a displacement-controlled test would imply that the input would be the displacement in one or more nodes of the structure. In this experiment, despite the loads being applied considering the stress in each cable (with the load cells), the setup is not load-controlled because these loads are caused by the strain in each cable and this strain depends on the deformation of the structure, decreasing as the displacements occur, because the distance between the grip hoists and the structure decreases. It is not deformation-controlled, either, because each stage of the experiment is not set to achieve a target displacement—that is, the displacements are a consequence of the load.

This load system, characterized by a decrease in load due to an increase in displacements, allowed the experiment to continue after the maximum load capacity was reached, enabling the capture of the loading decrease (softening) stage of each structure.

Regulations and design of test structures

The design of the test structures complied with Eurocode 2, Eurocode 7, and Eurocode 8. Due to testing limitations regarding not only the maximum capacity of the grip hoists, but also concerning the costs of the foundations and anchor block, an adaptation was made: the longitudinal reinforcement of the columns had to be reduced and does not fully comply with Eurocode 8's requirements regarding the formation of plastic hinges in the beams at column-beam joints. Despite this, it was experimentally verified that the hinges occurred first in the beams, as initially intended. The design stage had to guarantee the following conditions: a ductile behavior (structural collapse caused by flexural failure at the bottom of the columns), the technical and

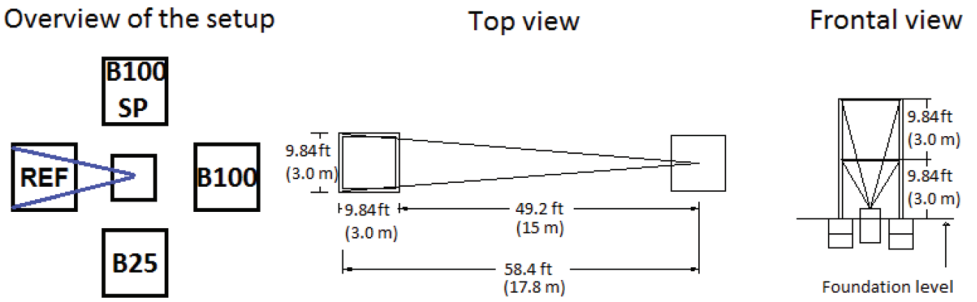

Fig. 2—Configuration of test setup.

Table 3—Load setup

Ratio between horizontal forces in upper cables and lower cables: 2.05				
Cable	Vector direction	Length, m (ft)	%/direction	Normalized force
Cable 1	Pushover	17.05 (55.92)	95.36%	205.00
	Orthogonal/horizontal	1.40 (4.59)	7.83%	16.83
	Orthogonal/vertical	5.20 (17.06)	29.08%	62.52
Cable 2	Pushover	18.76 (61.53)	96.12%	205.00
	Orthogonal/horizontal	1.40 (4.59)	7.17%	15.30
	Orthogonal/vertical	5.20 (17.06)	26.64%	56.82
Cables 3 and 4	Pushover	18.00 (59.04)	99.07%	100.00
	Orthogonal/horizontal	1.13 (3.71)	6.19%	6.25
	Orthogonal/vertical	2.20 (7.22)	12.11%	12.22

economic feasibility of the experiment, and a simple test setup that would guarantee the operation of the equipment without errors.

Due to the reduction of the longitudinal reinforcement of the columns, these elements are moderately reinforced, with a geometric ratio of reinforcement of 1.3%, between 1% and 4% (the reinforcement ratio values recommended by Eurocode 2); and the collapse of the cross sections is achieved by steel failure, rather than concrete failure after steel yielding. According to codes and regulations, both of these collapses are desirable, ensuring ductility and a proper use of the materials. This fact has a slight influence on the performance of the structures, which was not considered significant because only the performance after steel hardening is affected. Nevertheless, the fact that the behavior of the cross sections involved in the collapse mechanism was not characterized by concrete failure should be taken into consideration when comparing the precollapse behavior of the concrete mixtures.

The computer program used was CSI's SAP2000 (v15) and the loads were applied considering the geometry of the structure and an inverted triangular horizontal distribution, with loads applied to both floors at the slab level. Table 3 shows such forces, applied in nodes as a "displacement-controlled load case". This kind of load is defined as a vector (last column of the table), and for each step, the software applies a factor that increases or decreases the forces (during loading or unloading stages) in comparison with the previous load step.

For the purpose of designing the test setup, the finite element model (FEM), used for both the structures and the anchor block (as well as the rest of the load application system), was made considering the concrete's (Class C25/30) 95% characteristic material properties, instead of the normally used 5% characteristic values. The material characteristics of the reinforcement steel were, at this stage, estimated considering that the yielding stress was 1.3 times the characteristic design value (the maximum capacity specified by Eurocode 2). The nonlinearities were modelled as fiber plastic hinges (at the ends of the columns and beams), and the model suggested by *Mander et al.* (1988) was used to estimate the properties of confined concrete. The maximum forces of the cables during the experiment, predicted by the FEM, were used to design the anchor block; Eurocode 7 was taken into consideration, and possible undesired collapse mechanisms (such as shear failure of the structural elements or toppling) were accounted for and avoided.

The anchor block was 5.76 ft (1.70 m) high, 3.94 ft (1.20 m) of those sunken into the ground (mobilizing passive soil pressure) and has a square shape with 9.02 ft (2.75 m) of side. A grid of reinforcement bars was used as well as a system with 3.28 ft (1.00 m) screws and threaded couplers, which allowed the attachment of the bi-articulated anchor points.

Model's characterization

Figure 3 shows the model's geometry and reinforcement layout. The slabs were 3.94 in. (0.10 m) thick and their reinforcement had a bottom mesh of 0.315 in. (8 mm) reinforcing bars spaced 7.87 in. (200 mm) in both directions. Because the foundations (Fig. 4) are two large concrete blocks, a full base restraint of the columns is ensured (as confirmed during the tests by the displacement values of topographic targets 5 and 6). The reinforcing bar cover in the columns is 0.98 in. (25 mm) and, in the rest of the structure, 0.79 in. (20 mm).

A geometry survey of each structure was performed and the actual dimensions of the structures were known: the slabs' thickness ranged between 0.34 and 0.38 ft (104 and 116 mm) and the columns' cross section sides varied between 0.64 and 0.72 ft (195 and 219 mm). The density of each concrete mixture was considered equal to the average of those of 16 standard test cubes, made during the execution of each of the structures.

These dimensions and densities were used for finite element modeling purposes. The FEM used in each structure also considered the results of laboratory tensile tests on reinforcing bars from the same batch as the reinforcing bars used on site, the results of laboratory tests on concrete samples produced in laboratory and of concrete cores taken from the structures, and the results of the dynamic characterization tests (Pacheco et al. 2015). A pushover curve for each structure was obtained. Figure 5 shows the numeric pushover curve of the REF structure.

Test procedure

The structures were tested on two consecutive days. A data logger and four tension load cells were used to measure the

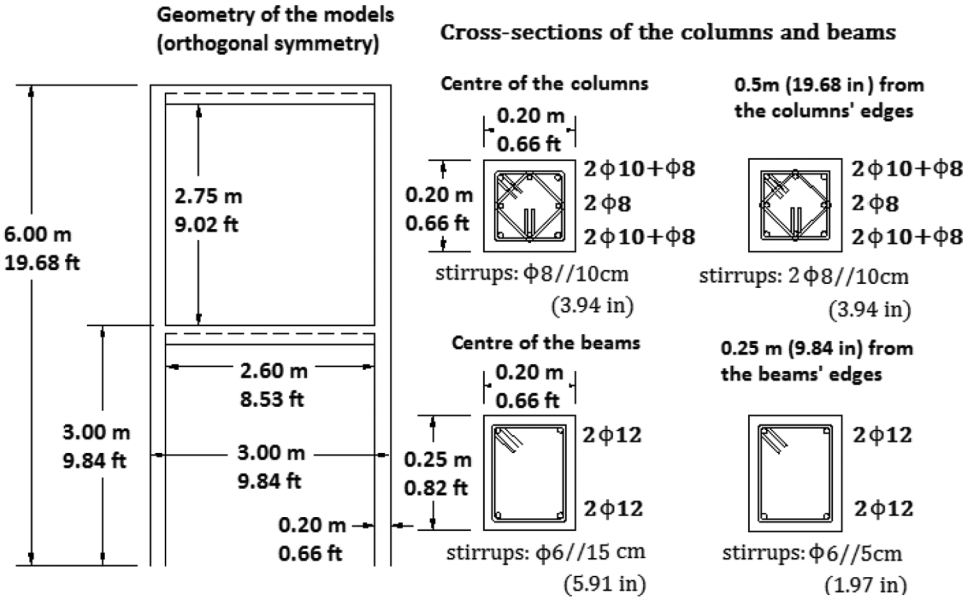

Fig. 3—Geometry and reinforcement layout of test structures.

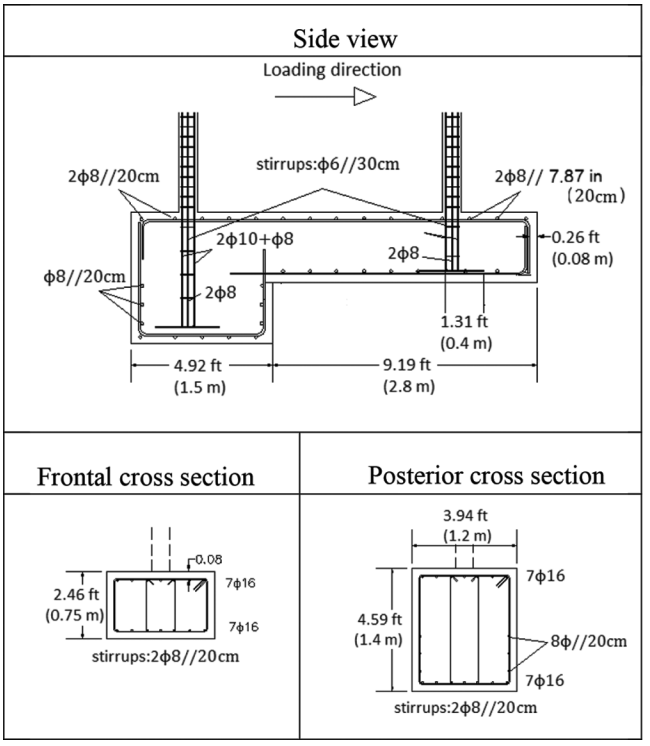

Fig. 4—Geometry and reinforcement layout of foundations.

loads applied by each cable, ensuring a load application in accordance with the distribution shown in Table 3. A digital inclinometer was used to measure the angles of the cables and of the load cells with the horizontal, to account for the loads effectively applied in the direction of the pushover experiment (horizontal).

The load was applied in increments/decrements of 1.12 kip (5 kN) and at the end of each step, the displacement of the topographic targets was measured. When cracks started to appear in the lower half of the two columns tensioned by the cables, crack width measurements were registered, as well as the crack spacing at the end of the experiment. Most of

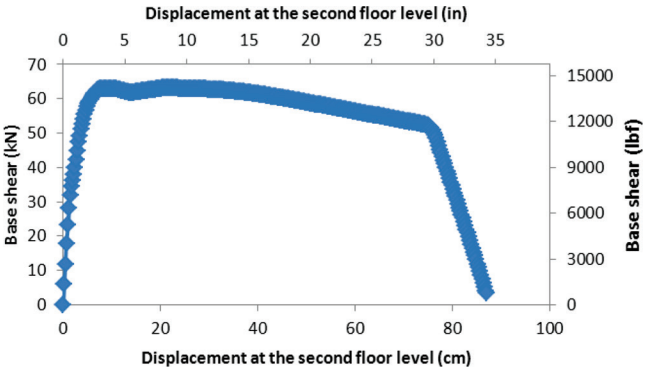

Fig. 5—Numeric pushover curve: REF structure.

the topographic targets placed at the column-beam joints at the first floor level of the structures could not be used at the final stages of the experiment, due to the loss of the concrete cover they were attached to. The same phenomenon, caused by the lower strain capacity of the concrete cover (unconfined), occurred at the bottom of the columns. Figure 6 shows some details of the experiment.

RESULTS AND DISCUSSION

Behavior of the structures

The behavior of the structures followed the same pattern, thus, only the behavior of one of them (B100) will be described in detail.

Because the purpose of the topographic targets 5 and 6 was to confirm the total restraint of the foundations as well as the absence of toppling (both confirmed), no further mention of their measurements is made.

Herein, the forces applied by the cables concern the forces in the direction of the experiment, after the decomposition of the values registered by the load cells.

The behavior of the test structures followed the prediction of the FEM's, both in terms of deformations and forces. Figure 7 shows the displacement at the second-floor level caused by forces and corresponding moments (at ground

Fig. 6—Some operations during one test.

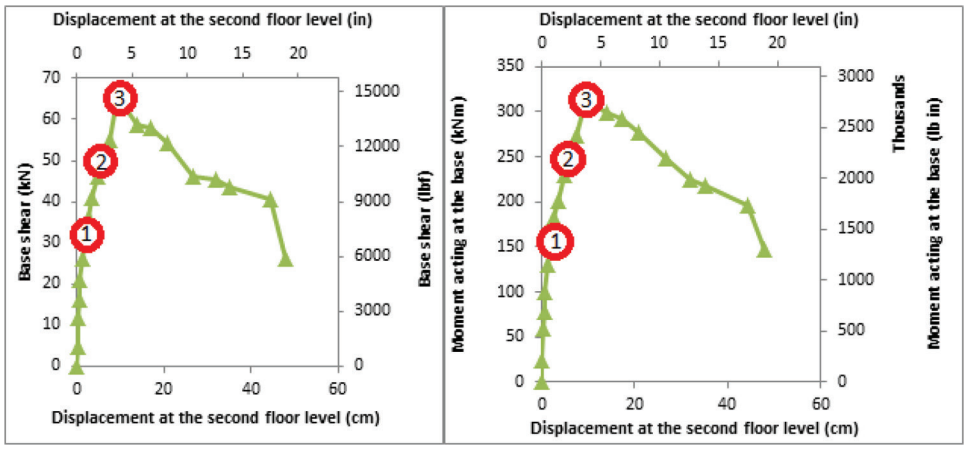

Fig. 7—Experimental load-deformation curves: B100 structure.

level). This figure and Table 4 allow a comparison between the experimental load distribution and the intended inverted triangular distribution shown in Table 3.

Cracking of the columns was noticed only after these elements reached relevant deflections (Stage 1 in Fig. 7). The structural yielding (Stage 2) was caused by basal forces of approximately 11,240 lbf (50 kN), corresponding in the FEM to a bending moment at the bottom of the columns of 14751 lbf-in. (20 kN-m). The yielding bending moment of those sections had been algebraically estimated at the cross section level as 15,341 lbf-in. (20.8 kN-m).

The maximum experimental loading capacity, Stage 3 in Fig. 7, is 14,837 lbf (66 kN). This value is close to the FEM prediction—14,163 lbf (63 kN). The bending moment at the bottom of the tensioned columns associated to this base shear, 19,398 lbf-in. (26.3 kN-m), is also close to the algebraic estimation of the maximum cross section bending capacity, when the hardening of the reinforcing bars and the axial force on the columns, 1124 lbf (5 kN), are considered—18,294 lbf-in. (24.8 kN-m).

In terms of qualitative behavior, a ductile behavior was observed with a significant post-yielding behavior (Fig. 8), mostly due to the detailing design. This shows that RA use is by no means a hindrance to proper ductile behavior, as long as conventional concrete code regulations are followed. The same figure clearly shows the failure mechanism: the structure collapses after flexural failure at the bottom of the ground-floor columns. Because the axial force acting on each column is expected to be low (in the FEM, the maximum value was lower than 1.12 kip (5 kN), the failure of the four columns (as well as any other behavioral stage) happens at the same time with approximately the same bending moment.

The hinge formation and collapse mechanism are shown in Fig. 9. After an initial behavior with no evident concentrated deformations in any cross section, the bottom of the ground-floor columns starts to have a significant curvature and exhibits cracks shortly afterward; at the same time, the two beams of the first floor parallel to the pushover direction also form plastic hinges, allowing the beams and slabs to remain horizontal, as Fig. 8 clearly shows. At this stage, the column-beam joints of the first floor rotate in agreement with the lower columns (also as shown in Fig. 9), and the upper columns show no evidence of plastic hinge formation but have a distributed curvature along their length that allows the upper beams and slab to remain horizontal with no hinge formation. The plastic hinges of the top of the columns of both stories only become visible on a third stage, characterized by higher rotations of the columns of the lower story (possibly due to the hinges on their top), when compared to

Table 4—Forces applied by each cable in pushover direction

	REF						B25						B100						B100SP					
	Forces in each cable																							
	Cable				Base shear, kN	Basal moment, kN-m	Cable				Base shear, kN	Basal moment, kN-m	Cable				Base shear, kN	Basal moment, kN-m	Cable				Base shear, kN	Basal moment, kN-m
Stage	1	2	3	4			1	2	3	4			1	2	3	4			1	2	3	4		
Visible cracking	8.1	10.9	4.9	4.5	28.4	142.2	9.8	9.3	3.8	4.6	27.5	139.8	9.7	10.3	5.3	5.7	31.0	153.0	9.7	10.2	4.6	3.7	28.2	144.3
Yielding	14.6	15.7	9.9	9.5	49.7	247.5	16.0	16.5	10.1	10.2	52.8	255.9	14.5	16.6	9.0	10.3	50.4	244.5	23.2*	15.8*	13.9*	14.8*	67.7*	320.1*
Maximum capacity	16.7	18.9	14.4	9.0	59.0	288.3	19.9	18.1	12.3	12.4	62.7	302.1	17.9	20.4	13.4	14.5	66.2	313.5	23.2	15.8	13.9	14.8	67.7	320.1
	Comparison between top/bottom cables (target ratio: 1.5)																							
Stage	Total top cables		Total bottom cables		Top/bottom		Total top cables		Total bottom cables		Top/bottom		Total top cables		Total bottom cables		Top/bottom		Total top cables		Total bottom cables		Top/bottom	
Visible cracking	19.0		9.4		2.02		19.1		8.4		2.27		20.0		11.0		1.82		19.9		8.3		2.40	
Yielding	30.3		19.4		1.56		32.5		20.3		1.60		31.1		19.3		1.61		39.0*		28.7*		1.36*	
Maximum capacity	35.6		23.4		1.52		38.0		24.7		1.54		38.3		27.9		1.37		39.0		28.7		1.36	
	Comparison between left/right cables (target ratio: 1.0)																							
Stage	Total left cables		Total right cables		Left/right		Total left cables		Total right cables		Left/right		Total left cables		Total right cables		Left/right		Total left cables		Total right cables		Left/right	
Visible cracking	13.0		15.4		0.84		13.6		13.9		0.98		15.0		16.0		0.94		14.3		13.9		1.03	
Yielding	24.5		25.2		0.97		26.1		26.7		0.98		23.5		26.9		0.87		37.1*		30.6*		1.21*	
Maximum capacity	31.1		27.9		1.11		32.2		30.5		1.06		31.3		34.9		0.90		37.1		30.6		1.21	

*In this structure, yielding stage was not clear.

Notes: 1 kN = 224.8 lbf; 1 kN-m = 8850.8 lb-in.

the rotation of the columns of the second story. The plastic hinges on the top of the columns of the second story allow the corresponding beams and slab to remain horizontal.

During the last stages of the test, concrete covers started to fail at the bottom of the columns due to lack of capacity of the unconfined concrete to withstand compressive strains in the same way as confined concrete, and at the column-beam joints of the first floor due to the different angles of the columns of the different stories.

Comparison between structures

Figure 10 shows that the load-displacement relations of the four structures were equivalent, showing no clear trends or noticeable influence of RA incorporation.

The apparent higher maximum base shear of structures B100 and B100SP is caused by a slightly different force distribution than intended (higher tension on the first-floor cables and lower tension on the second-floor cables, as shown in Table 4). As the bending moment-displacement curve shows, the maximum moments are identical in all the test-structures—maximum relative difference of 6% between these values and their average.

Because the failure of the columns is almost exclusively by bending, a rough correction of the basal forces, imposing the idealized 1.5 ratio between the forces of the top cables and the forces of the bottom cables and keeping the experimental maximum bending moment at the base of the structures, was made. This estimate gives "equivalent" maximum base shear forces of 59.8 kN (REF), 64.4 kN (B25), 60.5 kN (B100) and 61.4 kN (B100C50)—values with a maximum relative difference (to REF) of 7.7% (B25) and an average relative difference of 3.8%.

These results agree with most of the structural studies of the literature review; for most reinforced concrete structures, as long as proper design is performed (namely, by the mobilization of at least the yielding strain/stress capacity of the reinforcement steel), the load action-effects distribution depends mostly on the steel reinforcement, independent of RA incorporation. This is easily explained by looking at typical equations of the yielding or maximum moment of cross sections: the dependence on the concrete properties is hardly significant. Thus, it would be expected that differences would only be found in the precracking stage behavior of the structures, with higher deflections associated with B100, due to its lower modulus of elasticity (Pacheco et al. 2015). However, most probably due to shrinkage cracking of the REF structure, which reduced its equivalent stiffness, the REF's deflections were the highest.

Nevertheless, the deflections of the four structures did not differ significantly with relative differences to the reference structure of yielding displacements and displacements for maximum base shear below 12% and 20%, respectively. The relative difference of the B100SP structure at maximum base shear was higher (40%), for unknown reasons.

The experimental results, especially the fact that no RA incorporation trend was noticeable, show that the execution conditions are more relevant to the deformation behavior of the structures than the incorporation of these RA. The use of

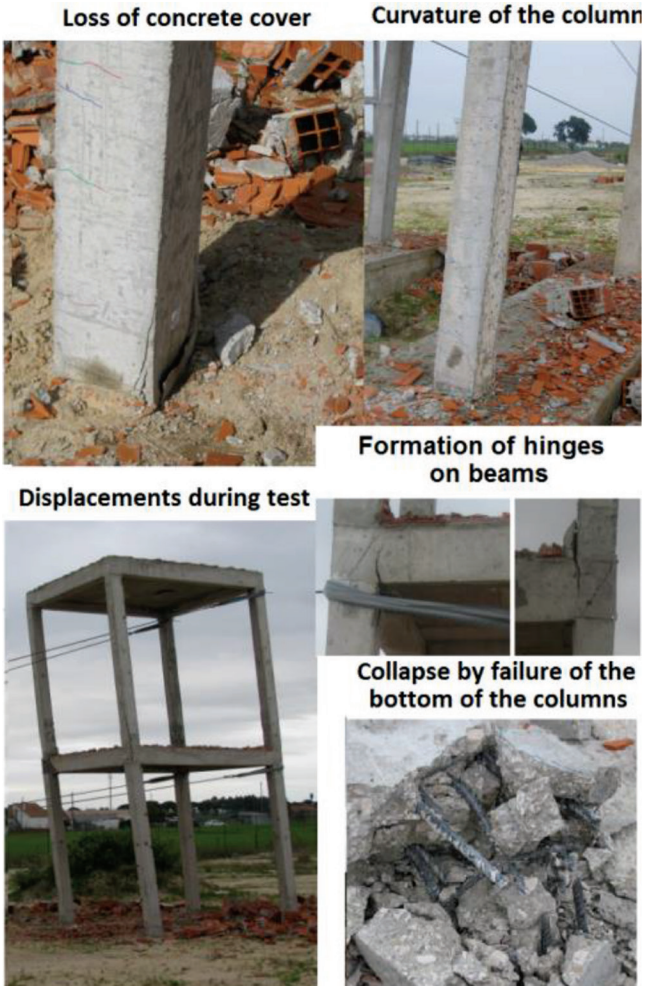

Fig. 8—Some details of behavior of B100.

RA was already expected to have a reduced effect, not only based on the results in the literature, but also because the FEM, which consider the in-place properties of the various concrete compositions, originated identical pushover results for the four structures in terms of shear capacity during the loading stage, as Tables 4 and 5 clearly demonstrate. In Table 5, the closeness between experimental and analytical base shear results is evident.

Because the experiment was not performed under controlled displacements (which was not a technically feasible option), the displacements and forces of each stage were conditioned by the load application system. To make the structures unload during the softening stage, it was necessary to slightly load them (by tensioning the cables) at each equilibrium stage. The unloading was then made by the dissipation system structure/cables, because the cables store a considerable amount of elastic energy. This produces additional displacements of the structures, decreasing the length and extension of the cables, thus reducing the load in each cable in comparison with the displacements and loads imposed in the beginning of each stage. This creates a difference between the numeric predictions and the experimental results, measured after the additional displacements of each stage occur.

This behavior is also relevant in the evaluation of the collapse displacements and loads. Because the precollapse

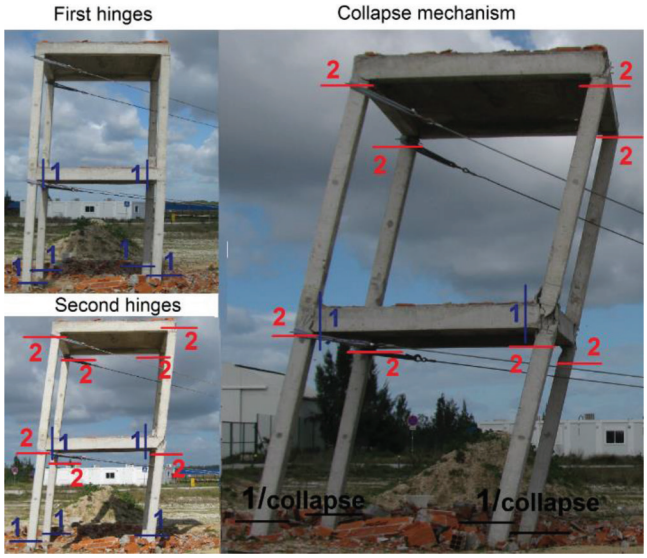

Fig. 9—Plastic hinge formation and collapse mechanism.

stages are associated with relevant structural damage, high displacements, and significant reductions in load capacity, the elastic energy of the cables leads to a premature collapse dependent on the execution of the experiment. If a grip hoist operator pushes the cable more quickly at a later stage of a structure's test, that structure will collapse for a lower horizontal displacement and a higher total base shear than the other ones.

Table 6 concerns the ductile behavior of the structures. Because the displacements at collapse depend on the test execution and no direct comparison can be made with a common ductility parameter $Duct._u$ (the ratio between collapse and yielding displacements), an additional ductility criterion was used for comparison, $Duct._{0.5}$ (the ratio between the softening displacement for half the maximum load capacity of the structure and the yielding displacement). The $Duct._{0.5}$ values in Table 6 show that RA has no significant effect on this parameter.

The comparison between Fig. 5 and Fig. 7 shows that the loading stage of the experiment followed the FEM's predictions quite well. The unloading stage results differ from expectations due to the aforementioned elastic energy stored in the cables.

Cracking

Crack width and spacing were measured at the lower half of the two columns tensioned by the cables. The load values associated with the different stages of cracking were also registered. For comparison purposes, the crack width at each load stage was considered as the average of three crack measures, while crack spacing was considered as the average of all the registered cracks of both columns of each structure after the collapse (typically approximately 17 quasi-horizontal cracks).

As Fig. 11 shows, Structures REF, B25 and B100SP had a similar behavior in crack spacing—variation between 3.9 and 4.3 in. (98 and 109 mm)—which suggests that RA incorporation did not influence this parameter significantly. Regarding crack opening, an erratic trend with high scatter

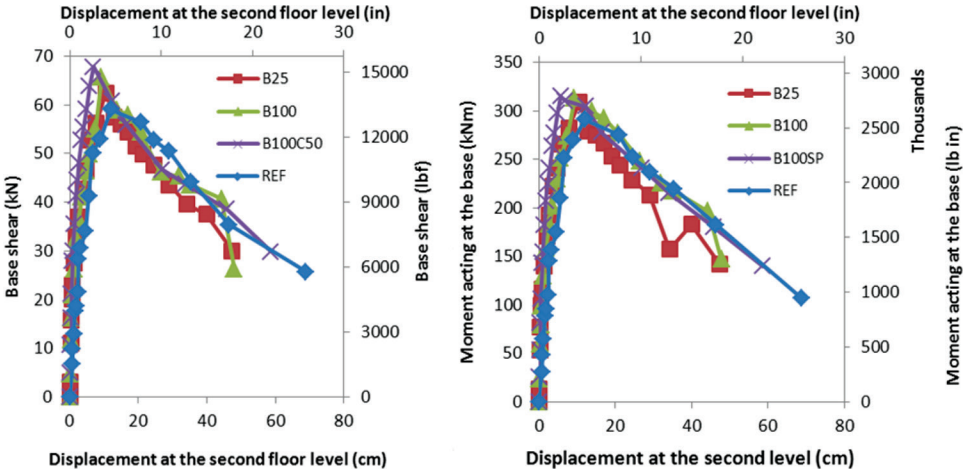

Fig. 10—Comparison between force-deformation curves.

Table 5—Experimental and numeric base shear values of each structural stage

Stage		REF	B25	B100	B100SP
Visible cracking	Experimental	6384 lbf (28.4 kN)	6182 lbf (27.5 kN)	6969 lbf (31.0 kN)	6339 lbf (28.2 kN)
	Numeric	—	—	—	—
Yielding	Experimental	11,173 lbf (49.7 kN)	11,869 lbf (52.8 kN)	11,240 lbf (50.0 kN)	15,219 lbf (67.7 kN)*
	Numeric	12,184 lbf (54.2 kN)	12,364 lbf (55.0 kN)	13,398 lbf (59.6 kN)	14,005 lbf (62.3 kN)
Maximum capacity	Experimental	13,263 lbf (59.0 kN)	14,050 lbf (62.5 kN)	14,882 lbf (66.2 kN)	15,219 lbf (67.7 kN)
	Numeric	14,207 lbf (63.2 kN)	14,162 lbf (63.0 kN)	14,297 lbf (63.6 kN)	14,972 lbf (66.6 kN)

*In this structure, the yielding stage was not clear.

Table 6—Ductility of each structure

Structure	REF	B25	B100	B100SP
δ_y	6.4	5.7	5.6	6.9
δ_u	66.0	47.4	48.0	58.8
$Duct._u$	10.3	8.3	8.6	8.5
$\delta_{0.5}$	57.0	46.1	46.3	52.6
$Duct._{0.5}$	8.9	8.1	8.2	7.6

(the confidence intervals in Fig. 11 were calculated for a 0.05 significance level) is observable. REF's cracks are noticeably narrower in comparison with the other structures, while B25's and B100's cracks were similar and B100SP's cracks stood roughly in between. This fact can be attributed both to the common scatter associated with the experimental study of this parameter and to possible undetected differences in concrete cover between structures.

Most of the studies in the literature review suggest that RA use results in higher crack widths and spacing, which are not in agreement with this study's findings.

This is explained not only by execution conditions (the structures were made in common construction conditions, instead of laboratory ones, which have a higher execution control), but also by the influence of reinforcement steel in the cracking behavior of concrete structures, as seen by González-Fonteboa and Martínez-Abella (2007). Because the columns of the test models have a low reinforcement spacing (as seen in Fig. 3) in comparison with the spacing of the beams of the studies cited in the literature review regarding cracking behavior, it was expected that any differences in cracking behavior due to RA would be significantly mitigated.

The crack spacing of the columns of the B100 structure is roughly 1.5 times that of the columns of the other three structures. This was an unexpected result because the tensile strength of all concrete mixtures was very similar according to the laboratory tests and there were no significant differences in terms of reinforcement cover. Because the B100SP structure had a cracking behavior similar to REF's and B25's, an explanation based on the loss of concrete/steel bond due to the material characteristics of the aggregates is not valid. Notwithstanding this fact, this deviating behavior can still be attributed to a loss in concrete/steel bond, but rather due to the higher apparent *w*/*c* of this mixture, than to the characteristics of the RA. It is, however, emphasized that this issue should be further developed and that the research of Guerra et al. (2014) and Butler et al. (2011) suggest that the incorporation of RA cannot be responsible for a reduction in concrete/steel bond that would originate such difference in concrete cracking. Therefore, the most probable cause for such a deviation from the behavior of the other structures is the execution conditions.

CONCLUSIONS

This experiment aimed at studying the applicability of recycled coarse aggregates and assessing the structural behavior of structures designed in compliance with Eurocode regulations. Full-scale models of three mixtures that

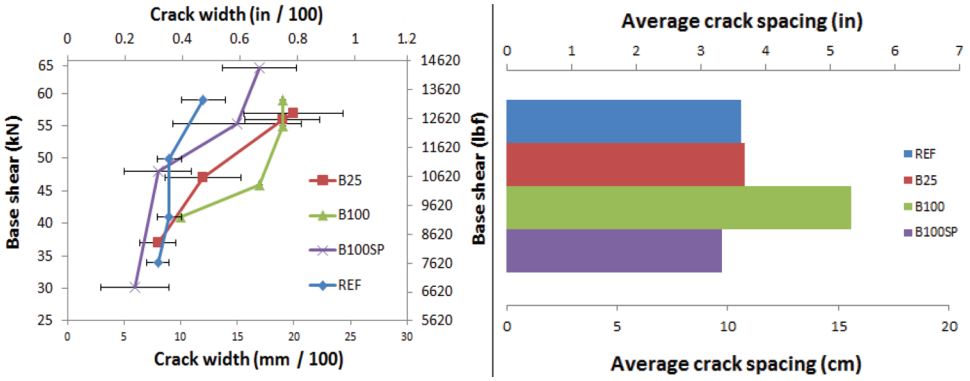

Fig. 11—Crack width and spacing.

included recycled aggregates, as well as a conventional concrete mixture, were produced and tested. The following conclusions can be drawn:

1. All structures behaved with the same pattern—that is, a ductile collapse mechanism;
2. The performance of each structure was correctly predicted by the corresponding FEM;
3. The load-deformation curves obtained were similar, with no clear impact of recycled aggregate incorporation;
4. The former conclusions are explained by the relevant role that reinforcement steel has on the ductile behavior of structures and on the ultimate and yielding internal forces of the cross sections;
5. Execution conditions are more relevant in the structural behavior than recycled aggregate incorporation;
6. Reinforcement steel is highly effective in reducing any possible detrimental effect of recycled aggregate incorporation in terms of cracking; and
7. If code regulations are followed and a proper design is made, the incorporation of high-quality recycled aggregates is no hindrance to a good seismic behavior of concrete structures made with them.

AUTHOR BIOS

João Pacheco *received his MSc in civil engineering from Instituto Superior Técnico (IST), Universidade de Lisboa, Portugal. His research interests include concrete science, structural concrete, and experimental testing.*

Jorge de Brito *is a Full Professor at IST, Universidade de Lisboa, where he received his MSc and PhD in civil engineering. His research interests include deterioration, rehabilitation, and management of concrete structures as well as sustainable construction.*

João Ferreira *is an Associate Professor at IST, Universidade de Lisboa, where he received his MSc and PhD. His research interests include experimental testing of structures and new composite materials.*

Diogo Soares *received his MSc in civil engineering from the IST, Universidade de Lisboa. His research interests include nondestructive testing and concrete science.*

ACKNOWLEDGMENTS

The authors gratefully acknowledge the support of Opway, IST, University of Lisbon, the ICIST Research Centre, and FCT (Foundation for Science and Technology). The authors also greatly acknowledge the support of the Portuguese Programme for Research and Development Associated with Public Contracts.

REFERENCES

Barbudo, A.; de Brito, J.; Evangelista, L.; Bravo, M.; and Agrela, F., 2013, "Influence of Water-Reducing Admixtures on the Mechanical Performance of Recycled Concrete," *Journal of Cleaner Production*, V. 59, pp. 93-98. doi: 10.1016/j.jclepro.2013.06.022

Bažant, Z. P., 1999, "Size Effect on Structural Strength: A Review," *Archive of Applied Mechanics*, V. 69, No. 9-10, pp. 703-725. doi: 10.1007/s004190050252

Björnström, J., and Chandra, S., 2003, "Effect of Superplasticizers on the Rheological Properties of Cements," *Materials and Structures*, V. 36, No. 10, pp. 685-692. doi: 10.1007/BF02479503

Butler, L.; West, J. S.; and Tighe, S. L., 2011, "The Effect of Recycled Concrete Aggregate Properties on the Bond Strength between RCA Concrete and Steel Reinforcement," *Cement and Concrete Research*, V. 41, No. 10, pp. 1037-1049. doi: 10.1016/j.cemconres.2011.06.004

Corinaldesi, V.; Letelier, V.; and Moriconi, G., 2011, "Behaviour of Beam-Column Joints Made of Recycled-Aggregate Concrete under Cyclic Loading," *Construction and Building Materials*, V. 25, No. 4, pp. 1877-1882. doi: 10.1016/j.conbuildmat.2010.11.072

EN 206-1, 2000, "Concrete—Part 1: Specification, Performance, Production and Conformity," Comité Européen de Normalisation, Brussels, Belgium, 72 pp.

Eurocode 2, 2004, "Design of Concrete Structures. Part 1-1: General Rules and Rules for Buildings (EN 1992-1-1 (2004))," European Committee for Standardization, Brussels, Belgium, 259 pp.

Eurocode 7, 2004, "Geotechnical Design. Part 1: General Rules (EN1997-1-1 (2004))," European Committee for Standardization, Brussels, Belgium, 179 pp.

Eurocode 8, 2004, "Design of Structures for Earthquake Resistance. Part 1: General Rules, Seismic Actions and Rules for Buildings (EN1998-1-1 (2004))," European Committee for Standardization, Brussels, Belgium, 229 pp.

Ferreira, L.; de Brito, J.; and Barra, M., 2011, "Influence of the Pre-Saturation of Recycled Coarse Concrete Aggregates on Concrete Properties," *Magazine of Concrete Research*, V. 63, No. 8, pp. 617-627. doi: 10.1680/macr.2011.63.8.617

Fonseca, N.; de Brito, J.; and Evangelista, L., 2011, "The Influence of Curing Conditions on the Mechanical Performance of Concrete Made with Recycled Concrete Waste," *Cement and Concrete Composites*, V. 33, No. 6, pp. 637-643. doi: 10.1016/j.cemconcomp.2011.04.002

Gonçalves, P., and de Brito, J., 2010, "Recycled Aggregate Concrete (RAC)—Comparative Analysis of Existing Specifications," *Magazine of Concrete Research*, V. 62, No. 5, pp. 339-346. doi: 10.1680/macr.2008.62.5.339

González-Fonteboa, B., and Martínez-Abella, F., 2007, "Shear Strength of Recycled Concrete Beams," *Construction and Building Materials*, V. 21, No. 4, pp. 887-893. doi: 10.1016/j.conbuildmat.2005.12.018

Guerra, M.; Ceia, F.; de Brito, J.; and Júlio, E., 2014, "Anchorage of Steel Rebars to Recycled Aggregates Concrete," *Construction and Building Materials*, V. 72, pp. 113-123. doi: 10.1016/j.conbuildmat.2014.08.081

Kou, S.-C.; Poon, C.-S.; and Wan, H.-W., 2012, "Properties of Concrete Prepared with Low-Grade Recycled Aggregates," *Construction and Building Materials*, V. 36, pp. 881-889. doi: 10.1016/j.conbuildmat.2012.06.060

Kwan, W. H.; Mahyuddin, R.; Kam, K. J.; and Sulieman, M. Z., 2012, "Influence of the Amount of Recycled Coarse Aggregate in Concrete Design and Durability Properties," *Construction and Building Materials*, V. 26, pp. 565-573.

Li, X., 2009, "Recycling and Reuse of Waste Concrete in China: Part II. Structural Behaviour of Recycled Aggregate Concrete and Engineering

Applications," *Resources, Conservation and Recycling*, V. 53, No. 3, pp. 107-112. doi: 10.1016/j.resconrec.2008.11.005

LNEC E 471, 2006, "Guide for the Use of Coarse Recycled Aggregates in Concrete with Hydraulic Binders," National Laboratory of Civil Engineering, Lisbon, Portugal, 7 pp. (in Portuguese)

Mander, J. B.; Priestley, M. J. N.; and Park, R., 1988, "Theoretical Stress-Strain Model for Confined Concrete," *Journal of Structural Engineering*, ASCE, V. 114, No. 8, pp. 1804-1826. doi: 10.1061/(ASCE)0733-9445(1988)114:8(1804)

Matias, D.; de Brito, J.; Rosa, A.; and Pedro, D., 2013, "Mechanical Properties of Concrete Produced with Recycled Coarse Aggregates—Influence of the Use of Superplasticizers," *Construction and Building Materials*, V. 44, pp. 101-109. doi: 10.1016/j.conbuildmat.2013.03.011

Olorunsogo, F. T., and Padayachee, N., 2002, "Performance of Recycled Aggregate Concrete Monitored by Durability Indexes," *Cement and Concrete Research*, V. 32, No. 2, pp. 179-185. doi: 10.1016/S0008-8846(01)00653-6

Pacheco, J.; de Brito, J.; Ferreira, J.; and Soares, D., 2015, "Dynamic Characterization of Full-Scale Structures Made with Recycled Coarse Concrete Aggregates," *Journal of Cleaner Production*, doi:10.106/j.jclepro.2015.08.45

Pereira, P.; Evangelista, L.; and de Brito, J., 2012, "The Effect of Superplasticisers on the Workability and Compressive Strength of Concrete Made with Fine Recycled Concrete Aggregates," *Construction and Building Materials*, V. 28, No. 1, pp. 722-729. doi: 10.1016/j.conbuildmat.2011.10.050

Poon, C. S.; Kou, S. C.; and Lam, L., 2002, "Use of Recycled Aggregates in Molded Concrete Bricks and Blocks," *Construction and Building Materials*, V. 16, No. 5, pp. 281-289. doi: 10.1016/S0950-0618(02)00019-3

Sato, R.; Maruyama, I.; Sogabe, T.; and Sogo, M., 2007, "Flexural Behavior of Reinforced Recycled Concrete Beams," *Journal of Advanced Concrete Technology*, V. 5, No. 1, pp. 43-61. doi: 10.3151/jact.5.43

Soares, D.; de Brito, J.; Ferreira, J.; and Pacheco, J., 2014, "Use of Coarse Recycled Aggregates from Precast Concrete Rejects: Mechanical and Durability Performance," *Construction and Building Materials*, V. 71, pp. 263-272. doi: 10.1016/j.conbuildmat.2014.08.034

Wang, C., and Xiao, J., 2013, "Study of the Seismic Response of a Recycled Aggregate Concrete Frame Structure," *Earthquake Engineering and Engineering Vibration*, V. 12, No. 4, pp. 669-680. doi: 10.1007/s11803-013-0205-x

Xiao, J.; Li, J.; and Zhang, C., 2005, "Mechanical Properties of Recycled Aggregate Concrete under Uniaxial Loading," *Cement and Concrete Research*, V. 35, No. 6, pp. 1187-1194. doi: 10.1016/j.cemconres.2004.09.020

Xiao, J.; Li, W.; Fan, Y.; and Huang, X., 2012, "An Overview of Study on Recycled Aggregate Concrete in China (1996-2011)," *Construction and Building Materials*, V. 31, No. 1, pp. 364-383. doi: 10.1016/j.conbuildmat.2011.12.074

Xiao, J.; Sun, Y.; and Falkner, H., 2006, "Seismic Performance of Frame Structures with Recycled Aggregate Concrete," *Engineering Structures*, V. 28, No. 1, pp. 1-8. doi: 10.1016/j.engstruct.2005.06.019

Yang, Y.-F., and Han, L.-H., 2006, "Experimental Behaviour of Recycled Aggregate Concrete Filled Steel Tubular Columns," *Journal of Constructional Steel Research*, V. 62, No. 12, pp. 1310-1324. doi: 10.1016/j.jcsr.2006.02.010

Yoshioka, K.; Sakai, E.; Daimon, M.; and Kitahara, A., 1997, "Role of Steric Hindrance in the Performance of Superplasticizers for Concrete," *Journal of the American Ceramic Society*, V. 80, No. 10, pp. 2667-2671. doi: 10.1111/j.1151-2916.1997.tb03169.x